ELSEVIER

PII: S0032-3861(97)10269-5

Polymer Vol. 39 No. 25, pp. 6473–6482, 1998

0032-3861/98/$ - see front matter

Heat induced shrinkage and microstructural changes in PET: As-spun fibres prepared via 'Controlled Threadline Dynamics'

Gang Wu[a,*], Takashi Yoshida[b] and John A. Cuculo[c]
[a]*College of Material Science and Engineering, Beijing University of Chemical Technology, Beijing 100029, China*
[b]*Division of Biological Sciences, Graduate School of Science, Hokkaido University, Sapporo 060, Japan*
[c]*Fiber and Polymer Science Program, College of Textiles, North Carolina State University, Raleigh, NC 27695-8301, USA*
(Received 23 July 1997; revised 29 October 1997; accepted 6 November 1997)

Macroscopic shrinkage behaviour and microstructural changes in PET as-spun fibres prepared by a normal cooling and by a 'Controlled Threadline Dynamics' (LIB)† process have been investigated as a function of temperature. For normally cooled spun fibres, the shrinkage and microstructural changes may be respectively divided into two steps with increasing temperature. A significant shrinkage in the low temperature range was attributed mainly to a disorientation process in oriented noncrystalline chains. In the higher temperature region, the still relatively high but gradually decreasing shrinkage is related principally to the diminished disorientation process and a sequential crystallization process. In comparison with the normally cooled spun fibres, a small but monotonically increasing shrinkage was found in the case of the (LIB) samples. Structurally, a monotonic increase in crystallinity and a decrease in fraction of oriented noncrystalline phase were found to accompany the shrinkage behaviour. This indicates that the microstructural change and corresponding shrinkage in the LIB spun fibres is a one-step process. The ultra-high oriented noncrystalline structure which results from the LIB process may promote minimization of distance between molecular chains in the oriented noncrystalline regime, and enhance intermolecular cohesive forces. When the fibres are heat treated, large-scale molecular motion may be restricted because of high intermolecular interaction. Instead, local thermal motion of highly stretched noncrystalline chains may be activated, and the conversion from very taut noncrystalline chains to a crystalline phase may be easier because of smaller intermolecular distances and enhanced cohesive forces. Therefore, the entire process may be characterized mainly as a continuous mass transfer from oriented noncrystalline phase to crystalline phase in situ, eschewing massive molecular recoiling. This may result in restricted disorientation in the noncrystalline phase and consequently accompanied by apparently restricted shrinkage.

(Keywords: poly(ethylene terephthalate); threadline modification; hot shrinkage)

INTRODUCTION

One of the most critical characteristics of oriented synthetic fibres is their dimensional stability at high temperatures. Hot shrinkage, determined mainly by the complicated inter-related factors extant during processing, is not only an important property affecting actual use, but it also reflects the various structural features which make up the oriented sample. Many studies have appeared reporting the dimensional and/or microstructural changes of semicrystalline poly(ethylene terephthalate) (PET) fibres occurring under various heating conditions[1–22]. Depending on the individual observation and structural model assumed, various interpretations of the thermal shrinkage behaviour occurring in PET oriented samples have been proposed.

Studies by Samuels and by Wilson on the role of oriented molecular chain motion in the shrinkage of drawn PET have shown that shrinkage is directly correlated with amorphous orientations[4,6]. They pointed out that the overall contraction involves a rapid initial stage which is associated with disorientation in the oriented amorphous regions. This disorientation is essentially responsible for the fibre length change, and regular chain folding is associated with a subsequent crystallization stage which need not involve any fibre length change. Another point of view was proposed by Dumbleton[1], Statton[3], and Kato[9]. In order to explain the increased intensity of low-angle X-ray scattering observed in the case of oriented and shrunk PET yarns, they suggested that shrinkage involves chain folding, e.g. chain folding is the basic mechanism of shrinkage.

Further, investigation of the thermal shrinkage behaviour of as-spun PET fibres as a function of fibre take-up velocity has been reported[11,12]. It was found that shrinkage increases with an increase in the spinning speed and reaches a maximum value at around 3000 m/min and then decreases with a further increase in speed. The increase has been attributed to increasing noncrystalline orientation, the decrease due to the onset of crystallization during spinning. The hot shrinkage of as-spun fibres prepared by high speed melt spinning is relatively high. For example, the shrinkage at *ca*. 100°C of fibre sample spun at 3000 m/min, is about

* To whom correspondence should be addressed
† These fibres so prepared have come to be known as (LIB) fibres since a liquid isothermal bath is used in the process.

60%[12]. As a result, heat treatment of such normally cooled/high speed spun fibres is usually required for most applications.

In brief, a conventional and generally accepted concept based on most investigations may be summarized by the statement that the shrinkage behaviour of oriented PET samples is strongly influenced by their specific morphology. Amorphous regions play a dominant role in the shrinkage process and at lower temperatures shrinkage is due primarily to disorientation of the amorphous region. The perfection of a crystalline structure is very important for the stability of molecular orientation. Only the orientation fixed in equilibrium crystallites can be thermodynamically stable[18].

In our previous research, PET fibre formation via high-speed melt spinning has been modified by applying a liquid isothermal bath along the spinline[23–29]. The spinning dynamics were changed from a process controlled by inertia and air drag forces to one controlled by an imposed liquid frictional drag. As-spun fibres prepared under optimum LIB operating conditions exhibit unique structural features. In a word, extremely high threadline stress may develop more highly taut molecular chains, while restricting the crystal growth process. This results in lower crystallinity and high overall orientation in the material. In other words, LIB as-spun fibre samples contain significant amounts of oriented noncrystalline (ON) phase[25–28]. Such a structure resulted in as-spun fibre possessing excellent mechanical properties, being comparable to those of commercial products from the conventional two-step process, at least at temperatures below the glass transition. On the other hand, even though the thermal response of LIB as-spun PET fibres has not yet been studied in detail, some of our earlier experimental results have shown that LIB spun fibres exhibit relatively low shrinkage compared with normally cooled as-spun fibres made at the same spinning speed when they were exposed to boiling water or hot air at 177°C. This is quite surprising, because in general, samples possessing high noncrystalline orientation are expected to show significant shrinkage based on the traditional point of view as mentioned earlier.

This article presents the results of continuing research based on our previous studies and examines hot shrinkage behaviour by thermal mechanical analysis, infrared, X-ray, and density measurements. The relationship between macroscopic fibre shrinkage and microstructural changes operative during exposure to the thermal process is then discussed for these LIB PET fibres.

EXPERIMENTAL

Sample preparation

Sample identifying codes and preparation conditions are given in *Table 1*. In order to compare the structural variation in the different PET fibres prepared with various processes, three types of samples were utilized. Samples A and B are conventional fibres spun with a normal cooling process at take-up velocities of 1500 and 3000 m/min. Samples C, D, and E are the LIB fibres. The preparation conditions of these fibres are exactly the same as those reported in our previous work[27]. A commercial tire cord yarn produced by the traditional two-step, e.g. spin/draw process was also used in this study as a reference sample, and was labeled F.

Characterization techniques

Dimensional change of the heated fibre samples was measured as a function of the temperature using a DuPont 1090 thermal mechanical analyzer (TMA). The heating rate during the TMA scan was 5°C/min and the pre-tension applied to the fibre bundle was *ca*. 0.2 MPa. Shrinkage was calculated according to the formula

$$\text{Shrinkage} = [(\text{initial length} - \text{final length})/(\text{initial length})] \times 100\% \quad (1)$$

In order to acquire a thorough understanding of the hot shrinkage behaviour of fibre samples, the potential microscopic mechanism was examined from the standpoint of conformation changes of molecular chains over a wide temperature range using infrared spectroscopy. The absorbance dependence of specific bands related to the *trans* and *gauche* conformers on the temperature variation were recorded on a Horiba 220 Fourier transform infrared (*FT*i.r.) spectrophotometer without directional preference. For *FT*i.r. spectral measurements under pre-tension at various temperatures, an optical cell developed by one of the present authors was used[30]. One end of the horizontally positioned sample was fixed in the holder and the other end was held taut by applying a weight. The load applied to the sample was 0.2 MPa which is equal to the pre-tension in the shrinkage measurement. The sample was heated by a surrounding heater programmed at a heating rate of 5°/min, heating of the sample started at *ca*. 30°C and *FT*i.r. measurements were made, starting at this temperature to *ca*. 200°C. This arrangement provided the same heating rate for both the hot shrinkage and the *FT*i.r. measurements. The comparison of the macroscopic shrinkage during the shrinkage test with the microscopic chain conformation change during the *FT*i.r. procedure is then more direct because we have minimized, if not removed, time effects.

To follow the fibre morphological changes with increasing temperature using X-ray crystallinity and density (by flotation), samples were heat treated under the same heating rate and pre-tension conditions as used in the TMA and *FT*i.r. measurements just described and then quenched in water at room temperature. Density and wide-angle X-ray scattering (WAXS) measurements on the above individual samples were then performed at room temperature, where it is assumed that the structures which existed at the end of the

Table 1 Preparation conditions of the fibre samples

Sample ID	Remarks	Take-up velocity (m/min)	LIB temp. (°C)	LIB depth (cm)	LIB position (cm)[a]
A	Normal cooling (without LIB)	1500	–	–	–
B	Normal cooling (without LIB)	3000	–	–	–
C	As-spun fibre prepared with LIB	1500	140	22	160
D	As-spun fibre prepared with LIB	3000	140	22	160
E	As-spun fibre prepared with LIB	5000	140	22	160
F	Commercial tire cord	–	–	–	–

[a]Position of LIB: distance between spinneret face and liquid surface

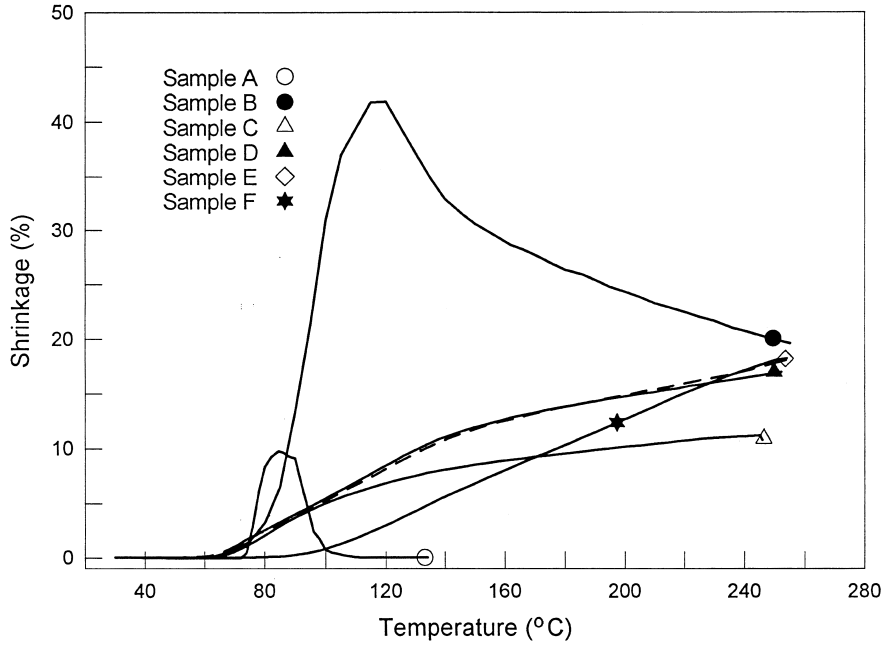

Figure 1 Temperature dependence of the shrinkage of various PET fibre samples

heating/quenching procedures survived. Fibre density was determined using a density gradient column filled with $NaBr/H_2O$ solution. WAXS scans were recorded with Ni-filtered CuK_α radiation generated at 30 kV and 20 mA.

Determination of the crystallinity of fibrous samples by WAXS requires that all preferred orientation of the fibres be eliminated. Fibres were finely cut and converted into powder-like isotropic samples to eliminate all preferred orientation.

The vibrational bands in infrared spectra and diffraction peaks in WAXS curves were fitted using the Pearson VII function, following the method introduced in refs [31,32].

RESULTS AND DISCUSSION

The percent thermal shrinkage of various PET fibres at constant load is plotted as a function of temperature in *Figure 1*. The dimensional change in all samples is low in the range below the glass transition, due to restricted molecular motion. Above T_g, the shrinkage increases significantly, but the traces of the various samples reveal obvious differences among themselves. For sample A wound at 1500 m/min under normal cooling conditions, only relatively low shrinkage was observed. It begins from *ca*. 70°C and ends at 100°C. The maximum shrinkage is only 10%. With further increase in temperature, the dimensional change becomes zero again, indicating that sample A with both low noncrystalline orientation and low crystallinity[27] has become an isotropic material through the heat induced disorientation during the shrinkage test. As spinning speed increases to 3000 m/min, a significant dimensional change is observed in sample B. In the pertinent literature covering fibre structural changes as a function of spinning speed under normal cooling conditions, it has been reported that PET fibres spun at 3000–4000 m/min contain a higher oriented amorphous phase than fibres spun at other speeds, and that they exhibit quite high hot shrinkages[11,12,32]. As seen in *Figure 1*, the shrinkage maximum occurs at *ca*. 40% in sample B. and the peak appears in the vicinity of 110–120°C. These results are in agreement with other reports, although the absolute values may vary somewhat. In the high temperature range ($T > 120$°C), the disorientation of oriented noncrystalline chains in this fibre has been almost completed, and only crystallization phenomenon occurs, resulting in a decreasing shrinkage. In comparison with the extremely high shrinkage peak obtained in this sample, the LIB spun fibres and tire cord yarn exhibit much smaller dimensional changes when subjected to high temperatures. The onset of the shrinkage in the tire cord yarn F was shifted to higher temperature and the percent shrinkage is seen to be lower than most of the other samples at corresponding temperatures. This may be attributed to its high crystallinity achieved by the hot drawing/heat setting process. For the LIB as-spun fibres, however, their excellent shrinkage behaviour is unexpected. As seen in *Figure 1*, the shrinkage traces of the three LIB fibres are similar to that of sample F, but they are obviously different from sample B. For example, fibre D reveals a much lower shrinkage than does fibre B at the same temperatures, although they were both wound at the same velocity of 3000 m/min. Another difference between sample Band LIB spun fibres is that the latter exhibit an increasing shrinkage in the high temperature range ($T > 120$°C) while sample B shows a decreasing trend as mentioned above. This is considered to occur by a continuous disorientation in the LIB spun fibres in the high temperature range. In a previous study, we have found a correlated phenomenon by dynamic mechanical analysis[27]. In comparison with a relatively narrow tan δ peak exhibited in normally cooled spun fibre, the LIB spun fibre exhibits a broader tan δ peak. Broadening of the glass transition in LIB spun fibre suggests an increase in the variety of noncrystalline chains, which exhibit different mobilities and hence different activation temperatures. Such broader distribution of the activation temperature may correspond to a continuous, wider (expands near the melt point) spectrum of molecular disorientation in a heated LIB spun fibre. Therefore, a monotonically increasing shrinkage in the LIB fibre was observed. *Table 2* shows the hot shrinkage data of PET fibres spun at 3000 m/min for both the normal cooling and the LIB process, in boiling water and 177°C hot air, derived from the literature and *Figure 1*. The data reported by our group (refs [26,33,34,39,40] and this work) are generally

Table 2 Hot shrinkage data and noncrystalline orientation content reported in the literature and for this work, for fibre samples spun at 3000 m/min under normal cooling and under ''Controlled Threadline Dynamics'' (LIB)

Normal cooling (without LIB)			Threadline modification (with LIB)		
In boiling water (%)	177°C hot air (%)	X_{ON} (%)	In boiling water (%)	177°C hot air (%)	X_{ON} (%)
28[26], 27[33], 32[40], 40[34], 60[35], 66[36], 73[37]	27[a], 46[12], 72[38] (at 150°C)	15[32]	9[33], 13[39], 12[40]	14[a], 20[26]	58[27]

[a]This work: the test procedure used in this instance differs from the standard ASTM D885, in that the sample is exposed to heat longer and become partially heat set

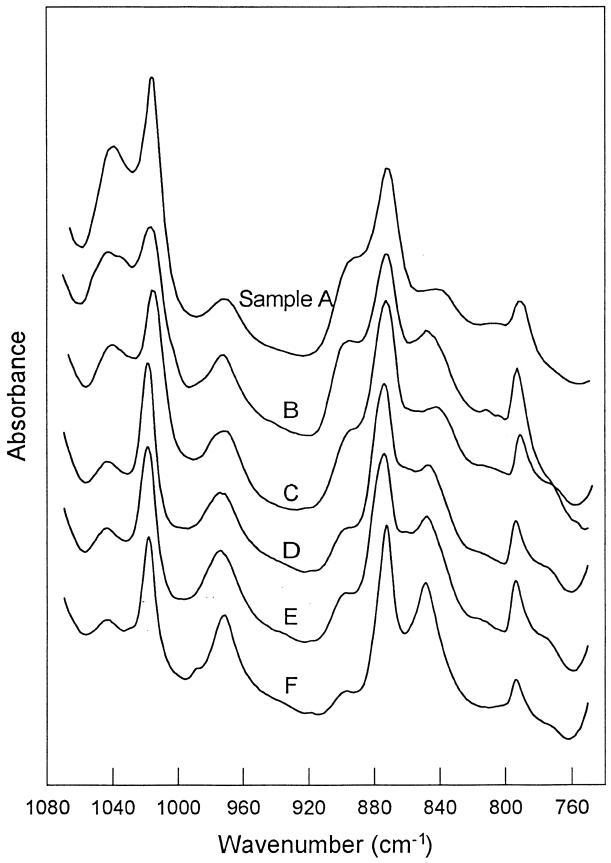

Figure 2 *FT*i.r. spectra for various fibre samples at room temperature

lower than those of others, because of the high molecular weight PET (IV $\approx$ 1.0 dL/g) used in our studies[33]. At the present time, no unequivocal explanation for this behaviour is at hand, but such materials may cause a higher spinline stress and induce a relatively higher crystallinity in the as-spun fibre, resulting in restricted, lower hot shrinkage than one observes in low IV fibres reported in other work. Ignoring this detail, *Table 2* reveals an important fact, e.g. the shrinkage of the LIB spun fibres determined in both boiling water and 177°C hot air is clearly lower than that of normally cooled samples. As pointed out in our previous works, one of the structural features of the LIB spun fibres is that they possess a high content of oriented noncrystalline phase[27]. As shown in *Table 2*, in comparison with 15% of oriented noncrystalline phase found in normally cooled fibre wound at 3000 m/min, the LIB spun fibre wound at the same velocity possesses a much higher content of anisotropic noncrystalline material (~58%). Based on conventional concepts, hot shrinkage is considered to be a disorientation process in the oriented noncrystalline phase with an accompanying increase in entropy. Thus, the higher the oriented noncrystalline content, the higher the expected hot shrinkage in a heating processing. However, the experimental data shown in *Figure 1* and *Table 2*, namely, samples C, D and E with high oriented noncrystalline content showing lower shrinkage than that of sample B which contains a lower oriented noncrystalline component, is a surprising result, and appears to conflict with conventional wisdom. To understand this unexpected macroscopic shrinkage behaviour, the microstructural changes including molecular conformation and crystallinity changes in LIB spun fibres during the heating process will be considered.

When the investigation is aimed at the molecular conformation changes, infrared spectroscopy is considered to be a useful tool. Infrared band assignments have been reported for the specific conformers, e.g. *trans* and *gauche*, and such bands have also been used to understand the structural changes that take place on spinning, drawing or annealing PET[31,41–43]. *Figure 2* shows *FT*i.r. spectra taken at room temperature for all six fibre samples A through F over the wavenumber region 760-1080 cm^{-1}. This zone is especially rich in confirmational information and very useful for analysis. In accord with refs [31,41,42], the bands near 845 and 970 cm^{-1} have been assigned to vibrational modes of the combined crystalline and amorphous *trans* ethylene glycol segment of the polymer chain. Bands near 899 and 1042 cm^{-1} have been assigned to vibrations of the *gauche* conformers which are taken to be present only in the isotropic amorphous phase. The 793 and 875 cm^{-1} bands have been associated with vibrations of the benzene ring and are not directly affected by conformational changes, hence these bands are usually used as internal reference bands. The changes in relative intensity of the *trans* and *gauche* bands, as observed in *Figure 2*, show clearly that different chain morphology exists in the six fibres. In general, at the same spinning velocity, the LIB spun fibres have a higher content of *trans* conformer than the normally cooled spun fibres, and are characterized by high total molecular orientation, as reported previously[25]. In order to examine the microstructural changes accompanying the macroscopic shrinkage, the temperature dependence of such specific vibrational bands was studied.

The *FT*i.r. spectra at increasing temperatures for two pairs of samples are shown in *Figures 3 and 4*. Here, the 845 cm^{-1} band and the 899 cm^{-1} band were chosen to represent the *trans* and *gauche* conformers, respectively. From these figures, one sees obvious differences in band intensity changes occurring in the various samples. In the case of the normally cooled spun fibres A and B (although the spectra of the latter become poorer because of significant fibre shrinkage at the higher temperatures), it is quite clear that a reverse in respective intensities of the *trans* and *gauche* bands occurs gradually with increasing temperature. In comparison with the normally cooled spun fibres, the relative intensity of *trans* and *gauche* bands in the LIB spun fibres C and D, especially in sample D, remains essentially

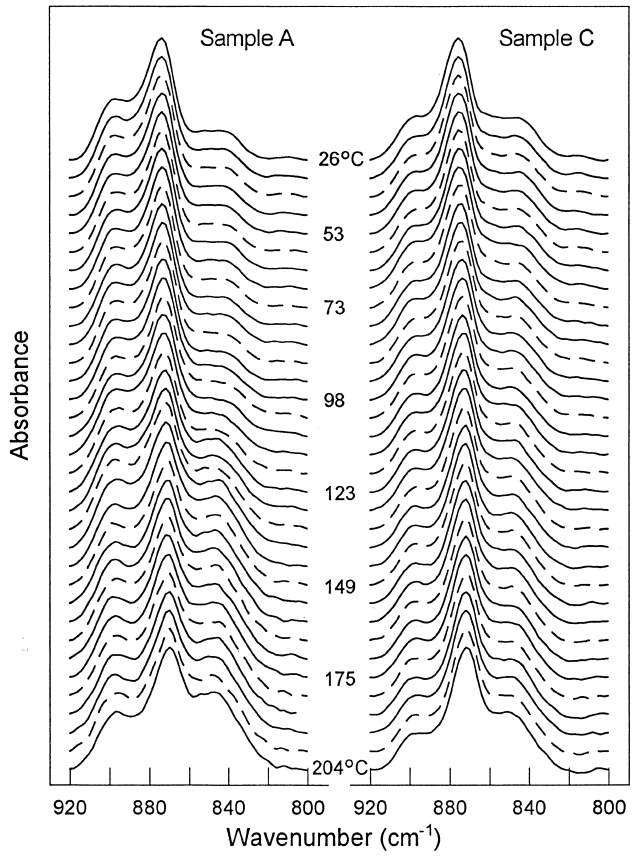

Figure 3 *FT*i.r. spectra of fibre samples A and C at various temperatures as indicated

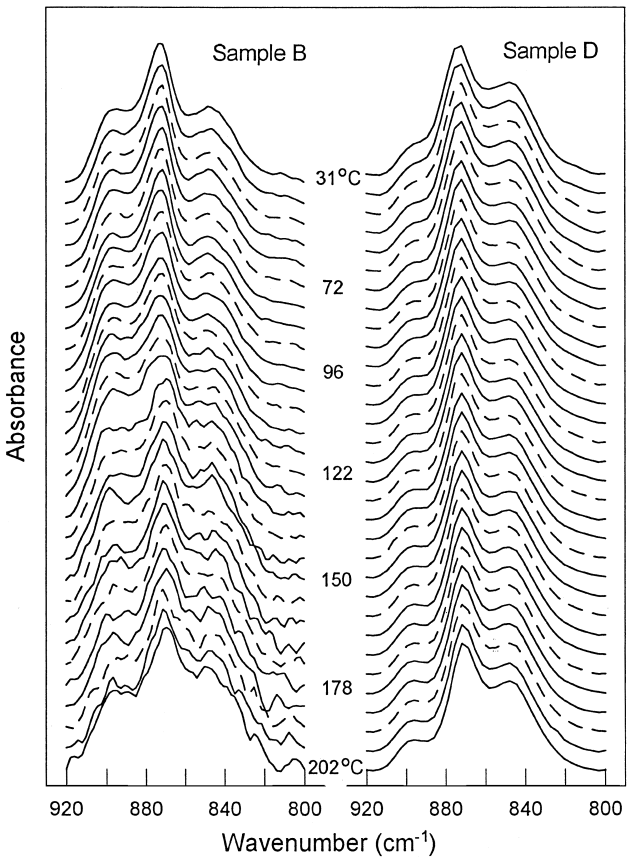

Figure 4 *FT*i.r. spectra of fibre samples B and D at various temperatures as indicated

constant with increasing temperature, indicating that only minor conformational change occurs within these fibres during the heating process. The observed infrared absorbance ratios A_{899}/A_{845} for each *FT*i.r. curve measured at different temperatures for the six samples are shown in *Figure 5*. A high value of the *gauche* to *trans* absorbance ratio can be considered indicative of a relatively high percentage of *gauche* conformations being present in a given sample.

As seen in *Figure 5*, changes in the A_{899}/A_{845} ratio due to the heating process are more obvious in samples A and B, where the ratio in both samples starts to increases from *ca*. 60°C, reaching a maximum, and then decreasing gradually with further increasing temperature to *ca*. 200°C. Such changes in the absorbance ratio present a clear implication, e.g. with increasing temperature, the content of the *gauche* conformer first increases, and then decreases with further increased temperature. The increase in this *gauche* content indicates a disorientation process and the decrease may be attributed to the crystallization process. This microstructural change observed in normally cooled spun fibres is consistent with conventional theory, and is also consistent with macroscopic shrinkage measurements. The maximum of the absorbance ratio may be indicative of the starting temperature of cool crystallization. It appears respectively at *ca*. 90°C and 120°C for samples A and B, and appears to be consistent with the peak positions on the shrinkage curves of the same samples as shown in *Figure 1*. On the other hand, the respective relative intensities of such conformation-sensitive bands for the LIB spun fibres C, D, E and tire cord yarn F reveal different tendencies. With increasing temperature, the absorbance ratio for sample C

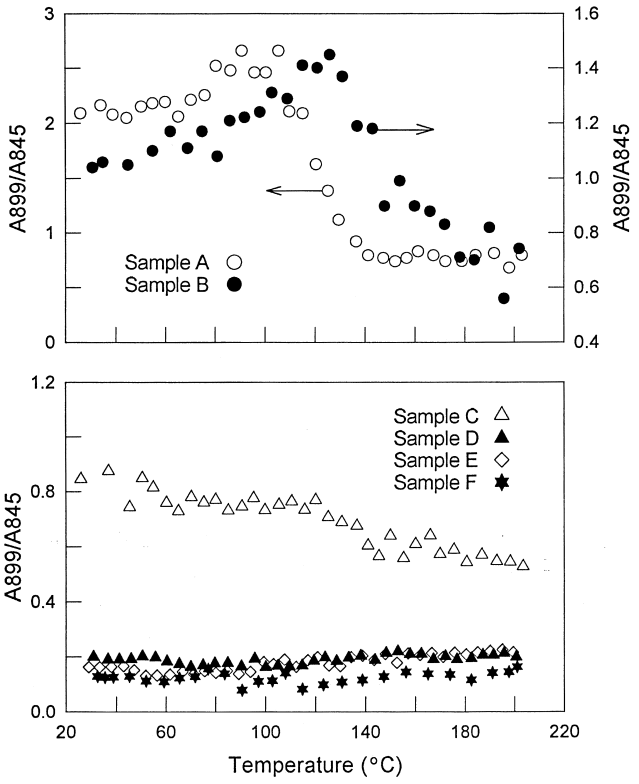

Figure 5 Temperature dependence of absorbance ratio (A_{899}/A_{845}) with ± 10% calculation error for various fibre samples

shows a slight, but monotonic decrease, while this same ratio for samples D and E seems to remain essentially constant over a wide temperature range as does the tire cord filament, although these two samples contain highly oriented noncrystalline phase[27]. This result indicates that no significant disorientation occurs in the oriented noncrystalline phase when these LIB spun samples were heated. A reasonable explanation appears to be that with increasing temperature, highly stretched noncrystalline chains may be converted directly into a crystalline domain. We call this suggested process 'in situ crystallization'. To confirm this hypothesis, however, further quantitative analysis of the morphological change occurring during the heating process is necessary. The problem raised here, more specifically, is to determine the temperature dependence of individual fractions of the *gauche* conformers in the isotropic amorphous phase (X_{IA}), and the *trans* conformers in both the crystalline (X_C) and the oriented noncrystalline (X_{ON}) phases. In order to attain this objective, a quantitative relationship between the relative areas of the *trans* and *gauche* bands and the total content of the *trans* conformers and *gauche* conformers must be established, remembering that *trans* conformers are present in both the crystalline and oriented noncrystalline phases; of course, the *gauche* conformer is formed only in the isotropic amorphous phase. In earlier work, Lin and Koenig had pointed out that the *trans* and *gauche* conformers are spectroscopically distinguishable by infrared analysis, and a relationship between the two conformers had been proposed as follows[42]:

$$T + G = 1 \tag{2}$$

with

$$T = T_a + T_c \tag{3}$$

where T is the total fraction of *trans* conformers, G is the fraction of *gauche* conformers, and T_a and T_c are the fractions of *trans* conformer in the noncrystalline and crystalline regions, respectively. Furthermore, for estimating the total fraction of the *trans* and *gauche* conformers in PET fibre samples with specific i.r. bands, Rodriguez-Cabello *et al.* proposed a method in which the oriented PET fibre was regarded as a two-phase conformational (not two-phase) model and the relationship between the relative areas of specific bands and the fraction of corresponding conformers is described by the follow equation[22]:

$$P_1(A_{trans}/A_{ref}) + P_2(A_{gauche}/A_{ref}) = 1 \tag{4}$$

where P_1 and P_2 are two coefficients to be determined related to the *trans* and *gauche* bands, and the values $P_1(A_{trans}/A_{ref})$ and $P_2(A_{gauche}/A_{ref})$ represent the *trans* and *gauche* conformer distributions, e.g. T and G, respectively. From equation (4) one obtains

$$(A_{ref}/A_{gauche}) = P_1(A_{trans}/A_{gauche}) + P_2 \tag{5}$$

If a pair of absorbance ratios of A_{ref}/A_{gauche} and A_{trans}/A_{gauche} can be determined for an individual fibre sample, the values of P_1 and P_2 may be determined by least-squares linear fitting.

In this study, the above described method was followed except that we choose 845 and 875 cm^{-1} bands as the *trans* and internal reference instead of 973 and 793 cm^{-1} bands used in ref [22]. With this modification, a common baseline can easily be drawn for a relatively narrow wavenumber range from 800 to 920 cm^{-1} which covers three meaningful peaks including 845, 875 and 899 cm^{-1} bands and overlaps with few meaningless bands. The accuracy of the peak fitting should be better. Therefore, equations (4) and (5) may be rewritten as:

$$P_1(A_{845}/A_{875}) + P_2(A_{899}/A_{875}) = 1 \tag{6}$$

and

$$(A_{875}/A_{899}) = P_1(A_{845}/A_{899}) + P_2 \tag{7}$$

According to the observed infrared spectra shown in *Figure 2*, both absorbance ratios A_{875}/A_{899} and A_{845}/A_{899} have been determined for the six samples by a peak fitting process. The experimental data for these samples are presented in *Figure 6*, where the few (six) data points are used to describe a straight line. The two coefficients were found to be:

$$P_1 = 0.96 \text{ and } P_2 = 1.39.$$

After determining the values of A_{845}/A_{875} and A_{899}/A_{875} for each *FT*i.r. scan shown in *Figures 3 and 4*, the fraction of the *trans* and *gauche* conformers at specific temperatures may be simply represented by the values of $P_1(A_{845}/A_{875})$ and $P_2(A_{899}/A_{875})$, respectively. It is worth noting again, that the term $P_1(A_{845}/A_{875})$ represents the 'total *trans* conformer' in both crystalline and noncrystalline regions. Our purpose, however, is to divide the total fraction of the *trans* conformers into its two components, and to determine their respective dependence on the heating temperature. This problem may be solved by combining the *FT*i.r. results with other characterizations such as WAXS or density measurements. For example, from the values of $P_1(A_{845}/A_{875})$ and the degrees of crystallinity (X_C) measured by the WAXS method, the *trans* fraction involved in the oriented noncrystalline region (X_{ON}) is given by:

$$X_{ON} = P_1(A_{845}/A_{875}) - X_C \tag{8}$$

considering

$$P_2(A_{899}/A_{875}) = X_{1A} \tag{9}$$

where X_{IA} is the relative fraction of the *gauche* conformers which exists only in the isotropic amorphous phase. Thus,

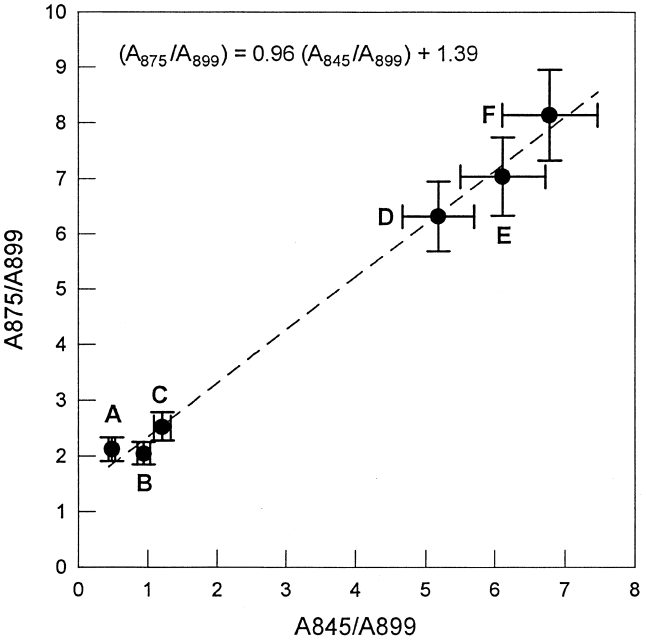

Figure 6 Plots of absorbance ratio A_{875}/A_{899} *versus* A_{845}/A_{899}, with ± 10% calculation error for various fibre samples

we have:

$$X_C + X_{ON} + X_{1A} = 1 \tag{10}$$

which is consistent with equations (2) and (3).

Figure 7 shows the WAXS scans performed at room temperature for powder-like samples of fibres B and D. In this measurement, as stated in the experimental section, fibre samples have been heated at a constant heating rate to the desired temperature indicated next to the WAXS curves, and then quenched. One sees that curves measured in the low temperature range for both samples have a broad diffuse scattering profile, indicating lower crystallinity or small crystallite sizes. Intensity curves in the higher temperature range, as expected, show fairly well-resolved diffraction peaks, indicating that a crystalline structure has been developed in both samples B and D. By careful observation, however, the temperature at which discreet peaks start to appear, due to crystalline growth, accompanied by diffraction peak narrowing, appears to be lower for sample D than sample B. In the d.s.c. results presented in a previous study[27], we have reported that the cold crystallization exothermic peak related to thermally induced crystallization during the heating process shifts to lower temperature with an increased fraction of the oriented noncrystalline phase. The observation found in *Figure 7* is considered to be consistent with the d.s.c. results. As the threadline tension is increased in the preparation of LIB spun fibres, the noncrystalline molecules would be extended more tautly than is the case in the conventional normally cooled spun fibre, resulting in the easing of the occurrence of cold crystallization and exhibiting the cold crystallization diffraction peak at a lower temperature.

From the values of X_{IA} and X_C determined respectively by *FT*i.r. and WAXS measurements, the fraction of the *trans* conformer in the oriented noncrystalline phase, e.g. X_{ON}, may be calculated by using equation (10). The percentages of each conformer, namely, X_{IA}, X_{ON}, and X_C are plotted *versus* temperature for samples B and D in *Figure 8*. Samples B and D were also subjected to density measurement in the same temperature range used for the *FT*i.r. and WAXS analysis. Plots of density as a function of temperature are given in *Figure 9*. Curves of density *versus* temperature for samples B and D are obviously different in relative values and shapes. Actually, Lin and Koenig had also proposed a formula relating the contents of the three types of conformers with density for PET samples[42]. The formula may be written as:

$$D_S = D_{IA}X_{IA} + D_{ON}X_{ON} + D_CX_C \tag{11}$$

where D_S is the density of the sample, D_{IA} is the density of the isotropic amorphous phase, and D_{ON} and D_C are the densities of the oriented noncrystalline and crystalline phases, respectively. They had also reported D_{IA}, D_{ON}, and D_C values for PET, as 1.326, 1.430 and 1.510 g/cm^3, respectively[42]. These values, however, appear to be too high. When used in the quantitative treatment of our density data, negative X_{ON} values were obtained. As a result, the density data shown in *Figure 9* are compared only qualitatively with other measured results at the present time, based on the assumption that $D_{IA} < D_{ON} < D_C$.

As shown in *Figure 8*, relatively low crystallinity (X_C) was found in both samples at room temperature, because of a relatively low take-up velocity of 3000 m/min. The values of X_{ON} and X_{IA} in the two samples vary drastically depending upon the preparation conditions. For sample D,

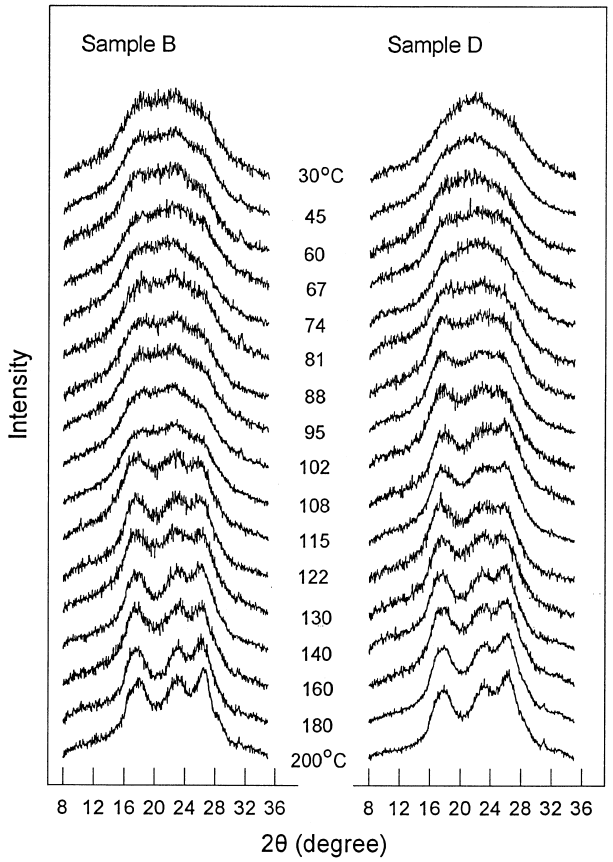

Figure 7 Wide-angle X-ray intensity curves of fibre samples B and D, at various temperatures as indicated

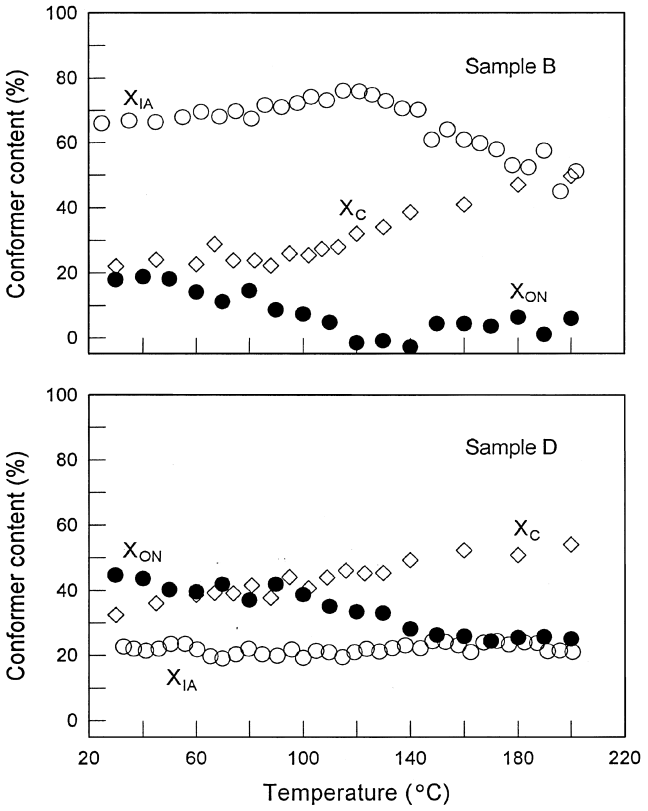

Figure 8 Relative conformer contents with ±10% calculation error for fibre samples B and D as a function of temperature

higher X_{ON} and much lower X_{IA} values are found compared with sample B. This may be attributed to the extremely high threadline tension encountered by sample D in the LIB process. In the case of sample B, an increasing X_{IA} accompanying a decrease in X_{ON} was found, as the temperature was elevated to 110–120°C. The crystallinity X_C remained almost constant in the same temperature range. Beyond 110–120°C, a significant increase in X_C and a drastic decrease in X_{IA} were observed, while the value of X_{ON} dropped close to zero. These results are consistent with the density data as well. As seen in *Figure 9*, the temperature dependence of density in sample B may be clearly divided into two segments on either side of 110°C. In the range below this critical temperature, density shows only a slight decrease which can be attributed to a decrease in X_{ON} and an increase in X_{IA} observed in the same region. For this sample, 110–120°C appears to be a critical temperature for initiating cold crystallization at the chosen heating rate (5°C/min). In the temperature range beyond the critical range, more and more molecular segments having the *gauche* conformation are converted continuously into a crystalline portion, resulting in a gradual increase in density. In comparison with sample B, the temperature dependence of the conformer content distribution and density for sample D shows obvious differences. As seen in *Figure 8*, the content of X_{IA} remains essentially constant with increasing temperature over the entire region, while decreasing X_{ON} is accompanied by an increasing X_C. This indicates that the precursors of the newly formed crystals come mainly from the highly oriented noncrystalline domain, namely the crystallization process occurs preferably in the oriented noncrystalline phase than in the isotropic amorphous phase. This is an essential distinction between sample D and sample B. In the latter, crystal formation is accompanied by a corresponding disappearance of the isotropic amorphous phase. Furthermore, unlike sample B, an elevation of X_C in sample D begins from quite a low temperature and there is a monotonic increase in its value without any sudden change in the temperature range shown. This may also be verified by the density data shown in *Figure 9*.

It is worth noting that, in our experience, it is difficult to obtain a unique fitting for the *FT*i.r. and WAXS data processing with current resolution programs. But usually, we were able to determine a rather reasonable range of fitted peak parameters. The results shown in *Figure 8*, therefore, are those we consider to be acceptable with an error of *ca.* 15%. Although this level of error is considered to be relatively high, the changing tendency of each fraction is supported qualitatively by density measurements and overall is considered to be a fair first approximation for explaining the macroscopic shrinkage behaviour.

Now, let us switch our attention to the original purpose of this study, that is, to explain the unexpected shrinkage phenomenon of the LIB as-spun fibres from the microstructural point of view. By combining observations extracted from independent measurements including *FT*i.r., WAXS and density, we attempt to distinguish the different shrinkage mechanisms occurring between the conventional normally cooled fibres and the LIB fibres. Based on the experimental results presented in *Figures 1, 8 and 9*, the hot shrinkage behaviour of conventional normally cooled as-spun fibre is regarded as a two-step process[4]. The first step refers to the heating process occurring from room temperature to about 110°C, whereas the second step begins at 110°C and ends at 200°C or higher. For sample B the temperature 110°C appears to be a critical turning point. All experimental observations, namely shrinkage, conformer content and density dependence on the temperature alter their respective behaviour at 110°C and show new and different dependency on temperature. In the first step, the disorientation of the oriented noncrystalline molecules occurs gradually. Such activated molecules tend to form domains of random coils, resulting in a decrease of X_{ON} and an increase of X_{IA}, with accompanying macroscopically significant shrinkage and reduced density. The recoiling process from a relatively straight molecular conformation may be accompanied by large-scale chain motion, inducing the high shrinkage observed in this region. In the vicinity of 110°C, the *trans* conformers in the noncrystalline phase have essentially disappeared, and a cold crystallization with

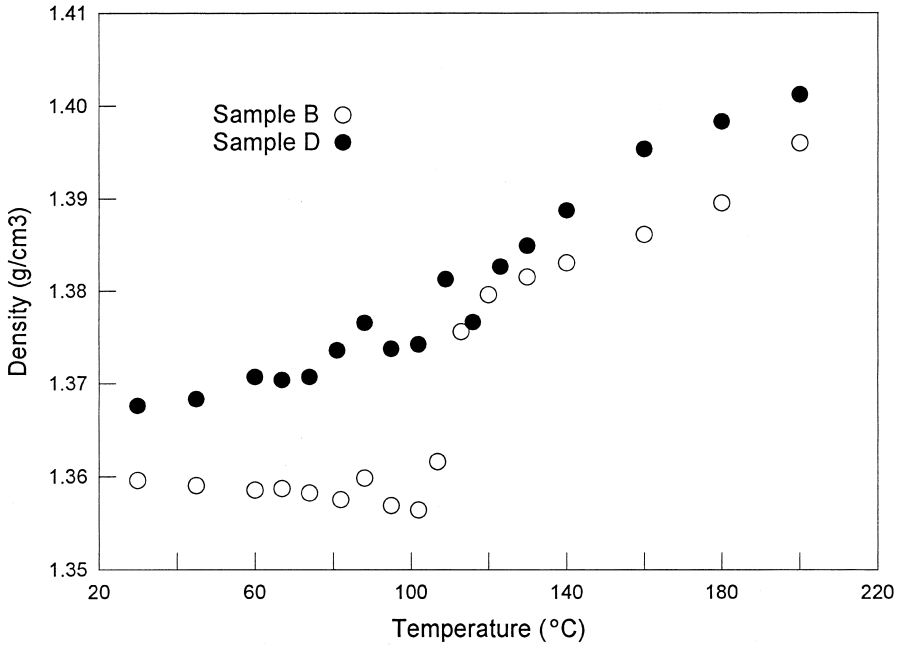

Figure 9 Temperature dependence of density of fibre samples B and D

gauche conformer consumption occurring gradually with further increasing temperature. These events result in a progressive decrease in amorphous content and a corresponding increase in both crystallinity and density. In comparison with the two-step mechanism found in normally cooled fibres, a one-step mechanism is proposed for the shrinkage process of LIB spun fibres based on the consistent observations of monotonic variation in shrinkage, conformer contents and density over the entire experimental temperature region studied. From the microscopic point of view, the entire process may be characterized as a continuous mass transfer from oriented noncrystalline phase to crystalline phase directly, skipping over the intermediate step—recoiled molecular conformation. This process may be described as 'in-situ crystallization'. In a kinetic study concerning microstructural changes occurring in heat treated PET fibres, Peszkin and Schultz have pointed out that hot shrinkage may be considered to be a competition between the chain recoiling process and the crystallization process[15]. Which process ultimately dominates will depend upon the original morphology of the as-spun fibre samples. As we have frequently pointed out, the most significant difference between normally cooled as-spun fibre and LIB as-spun fibre is the presence of an extremely highly oriented noncrystalline regime in the latter, which is caused by the extremely high threadline tension developed within the liquid bath. This unique morphology promotes minimization of distance between highly oriented molecular chains in the oriented noncrystalline domains, enhances intermolecular cohesive forces, and also promotes the so-called 'in-situ crystallization' which becomes relatively simple with only small-scale molecular motion involved. In a study on hot-drawing induced structural change in the LIB spun fibres, we have found that nearly fully developed structures, comparable to commercial PET tire cord, can be achieved with the application of a relatively small draw ratio (1.15–1.20) and minor heat treatments. These accumulated data lead us to hypothesize that the unique structure may cause an accelerated crystal development when it is subjected to heat treatment[28]. When such treatment is performed, large-scale molecular motion may be restricted because of high intermolecular interaction. Instead, high temperature may activate local thermal motions and permit the highly stretched, very taut noncrystalline chains (one-dimensional ordered phase) to be converted into a crystalline phase (three-dimensional ordered phase) in situ. The result being a significant transformation from highly oriented noncrystalline chains to an oriented crystalline phase by only one step.

CONCLUSIONS

In this study, macroscopic shrinkage behaviour and microstructural changes in PET as-spun fibres prepared by a normal cooling and by a Controlled Threadline Dynamics (LIB) process have been investigated as a function of temperature and compared with each other. The shrinkage of the threadline modified fibres is significantly restricted although they possess a considerably high noncrystalline orientation. This phenomenon at first appears to be in conflict with established convention, in which the shrinkage is generally predicted to increase with increasing content of the oriented noncrystalline phase. To explain this apparent contradiction, the corresponding microstructural changes, involving content dependence of the *trans* and *gauche* conformers was made using i.r., WAXS and density measurements. For the normally cooled spun fibre, the variation in conformer content may be divided into two steps. In the low temperature region where shrinkage starts from zero and reaches a maximum, increased X_{IA} and simultaneous decrease in X_{ON} were found, indicating that the significant shrinkage in the low temperature range is attributable mainly to a disorientation process in the oriented noncrystalline chains. In the higher temperature region, the reduced shrinkage which occurs may be related mainly to the crystallization process. These observations are consistent with established convention. In comparison with the normally cooled fibre, a small but monotonically increasing shrinkage was found in the case of threadline modified samples. Microscopically, a monotonic increase in X_C and a decrease in X_{ON} were found to accompany this shrinkage behaviour. This indicates that the microstructural change and corresponding shrinkage in the LIB spun fibres is a one-step process without chain disorientation in the oriented noncrystalline region. The unique morphology which results from the LIB process may promote minimization of distance between highly oriented molecular chains in the oriented noncrystalline regime, and enhance intermolecular cohesive forces. When heat treatment occurs, large-scale molecular motion may be restricted because of high intermolecular interaction. Instead, local thermal motion of highly stretched noncrystalline chains may be activated, and the conversion from very taut noncrystalline chains into a crystalline phase may be accelerated because of smaller intermolecular distance and enhanced cohesive forces. Therefore, the entire process may be characterized mainly as a continuous mass transfer from oriented noncrystalline phase to crystalline phase in situ. This may result in a restricted disorientation in the noncrystalline phase and a coincident, apparent restricted shrinkage.

ACKNOWLEDGEMENTS

G. Wu wishes to express his appreciation for the support from the National Natural Science Foundation of China (Grant No. 59673005) and Japan Society for the Promotion of Science (Grant No. 95030).

REFERENCES

1. Dumbleton, J. H., *J. Polym. Sci.*, 1969, **Part A-2**(7), 667.
2. Ribnick, A., *Text. Res. J.*, 1969, **39**, 742.
3. Statton, W. O., Koenig, J. L. and Hannon, M., *J. Appl. Phys.*, 1970, **41**, 4290.
4. Samuels, R. J., *J. Polym. Sci.*, 1972, **Part A-2**(10), 781.
5. Prevorsek, D. C., Tirpak, G. A., Harget, P. J. and Reimschuessel, A. C., *J. Macromol. Sci. Phys.*, 1974, **B9**(4), 733.
6. Wilson, M. P. W., *Polymer*, 1974, **15**, 277.
7. Nobbs, J. H., Bower, D. I. and Ward, I. M., *Polymer*, 1976, **17**, 25.
8. Bhatt, G. M. and Bell, J. P., *J. Polym. Sci. Part B: Polym. Phys.*, 1976, **14**, 575.
9. Kato, T., Yamamoto, Y., Saito, Y. and Kinoshita, S., *Sen-i Gakkaishi*, 1976, **32**, T279.
10. Buchanan, D. R. and Haudegree, G. L., *Text. Res. J.*, 1977, **47**, 732.
11. Shimizu, J., Okui, N., Kaneko, A. and Toriumi, K., *Sen-i Gakkaishi*, 1978, **34**, T64.
12. Heuvel, H. M. and Huisman, R., *J. Appl. Polym. Sci.*, 1978, **22**, 2229.
13. Gupte, K. M., Motz, H. and Schultz, J. M., *J. Polym. Sci. Part B: Polym. Phys.*, 1983, **21**, 1927.
14. Lin, S. B. and Koenig, J. L., *J. Polym. Sci. Part B: Polym. Phys.*, 1983, **21**, 2365.
15. Peszkin, P. N. and Schultz, J. M., *J. Polym. Sci. Part B: Polym. Phys.*, 1986, **24**, 2591.

16. Hristov, H. A. and Schultz, J. M., *J. Polym. Sci. Part B: Polym. Phys.*, 1990, **28**, 1647.
17. Long, S. D. and Ward, I. M., *J. Appl. Polym. Sci.*, 1991, **42**, 1921.
18. Trznadel, M. and Kryszewski, M., *J. Macromol. Sci., Rev. Macromol. Chem. Phys.*, 1992, **C32**(3 and 4), 259.
19. Peng, K. L. and Roland, C. M., *J. Polym. Sci. Part B: Polym. Phys.*, 1993, **31**, 1339.
20. Gupta, V. B., Radhakrishnan, J. and Sett, S. K., *Polymer*, 1994, **35**, 2560.
21. Goschel, U., *Polymer*, 1996, **37**, 4049.
22. Rodriguez-Cabello, J. C., Santos, J., Merino, J. C. and Pastor, J. M., *J. Polym. Sci. Part B: Polym. Phys.*, 1996, **34**, 1243.
23. Cuculo, J. A., Tucker, P. A. and Chen, G. Y., *J. Appl. Polym. Sci. Appl. Polym. Symp.*, 1991, **47**, 223.
24. Lin, C. Y., Tucker, P. A. and Cuculo, J. A., *J. Appl. Polym. Sci.*, 1992, **46**, 531.
25. Wu, G., Zhou, Q., Chen, J. Y., Hotter, J. H., Tucker, P. A. and Cuculo, J. A., *J. Appl. Polym. Sci.*, 1995, **55**, 1275.
26. Zhou, Q., Wu, G., Tucker, P. A. and Cuculo, J. A., *J. Polym. Sci. Part B: Polym. Phys.*, 1995, **33**, 909.
27. Wu, G., Jiang, J. D., Tucker, P. A. and Cuculo, J. A., *J. Polym. Sci. Part B: Polym. Phys.*, 1996, **34**, 2035.
28. Wu, G., Tucker, P. A. and Cuculo, J. A., *Polymer*, 1997, **38**, 1091.
29. Huang, B., Tucker, P. A. and Cuculo, J. A., *Polymer*, 1997, **38**, 1101.
30. Wu, G., Tashiro, K. and Kobayashi, M., *Macromolecules*, 1989, **22**, 188.
31. Heuvel, H. M. and Huisman, R., *J. Appl. Polym. Sci.*, 1985, **30**, 3069.
32. Shimizu, J., Okui, N. and Kikutani, T., in *High-Speed Fiber Spinning*, ed. A. Ziabiski and H. Kawai. Wiley Interscience, New York, 1985, Chap. 15.
33. Chen, G. Y., Ph.D. thesis, North Carolina State University, Raleigh, 1990.
34. Hotter, J. F., Ph.D. thesis, North Carolina State University, Raleigh, 1995.
35. Shimizu, J., Okui, N., Kikutani, T. and Toriumi, K., *Sen-i Gakkaishi*, 1978, **34**, T93.
36. Vassilatos, G., Knox, B. H. and Frankfort, H. R. E., in *High-Speed Fiber Spinning*, ed. A. Ziabiski and H. Kawai. Wiley Interscience, New York, 1985, Chap. 14.
37. Yasuzuka, K., *Sen-i Kikai Gakkaishi*, 1974, **27**, 275.
38. Hamidi, A., Abhiraman, A. S. and Asher, P., *J. Appl. Polym. Sci.*, 1983, **28**, 567.
39. Lin, C. Y., Ph.D. thesis, North Carolina State University, Raleigh, 1990.
40. Chen, J. Y., Tucker, P. A. and Cuculo, J. A., *J. Appl. Polym. Sci.*, 1997, **66**, 2441.
41. Miyake, A., *J. Polym. Sci.*, 1959, **38**, 479.
42. Lin, S. B. and Koenig, J. L., *J. Polym. Sci. Part B: Polym. Phys.*, 1982, **20**, 2277.
43. Gupta, V. B., Ramesh, C. and Siesler, H. W., *J. Polym. Sci. Part B: Polym. Phys.*, 1985, **23**, 405.